Inorganic Chemistry

Article

pubs.acs.org/IC

Magnetic Properties of Weakly Exchange-Coupled High Spin Co(II) Ions in Pseudooctahedral Coordination Evaluated by Single Crystal X-Band EPR Spectroscopy and Magnetic Measurements

Nicolás I. Neuman,[†] Elín Winkler,[‡] Octavio Peña,[§] Mario C. G. Passeggi,[†] Alberto C. Rizzi,[†] and Carlos D. Brondino*[,†]

[†]Departamento de Física, Facultad de Bioquímica y Ciencias Biológicas, Universidad Nacional del Litoral, S3000ZAA Santa Fe, Argentina

[‡]Centro Atómico Bariloche, CNEA- Instituto Balseiro, Universidad Nacional de Cuyo, San Carlos de Bariloche, Río Negro, Argentina

[§]Institut des Sciences Chimiques de Rennes, UMR 6226, Université de Rennes 1, 35042 Rennes, France

Supporting Information

ABSTRACT: We report single-crystal X-band EPR and magnetic measurements of the coordination polymer *catena*-(*trans*-(μ_2-fumarato)tetraaquacobalt(II)), **1**, and the Co(II)-doped Zn(II) analogue, **2**, in different Zn:Co ratios. **1** presents two magnetically inequivalent high spin $S = 3/2$ Co(II) ions per unit cell, named A and B, in a distorted octahedral environment coordinated to four water oxygen atoms and *trans* coordinated to two carboxylic oxygen atoms from the fumarate anions, in which the Co(II) ions are linked by hydrogen bonds and fumarate molecules. Magnetic susceptibility and magnetization measurements of **1** indicate weak antiferromagnetic exchange interactions between the $S = 3/2$ spins of the Co(II) ions in the crystal lattice. Oriented single crystal EPR experiments of **1** and **2** were used to evaluate the molecular **g**-tensor and the different exchange coupling constants between the Co(II) ions, assuming an effective spin $S' = 1/2$. Unexpectedly, the eigenvectors of the molecular **g**-tensor were not lying along any preferential bond direction, indicating that, in high spin Co(II) ions in roughly octahedral geometry with approximately axial EPR signals, the presence of molecular pseudo axes in the metal site does not determine preferential directions for the molecular **g**-tensor. The EPR experiment and magnetic measurements, together with a theoretical analysis relating the coupling constants obtained from both techniques, allowed us to evaluate selectively the exchange coupling constant associated with hydrogen bonds that connect magnetically inequivalent Co(II) ions ($|J_{AB}^{1/2}| = 0.055(2)$ cm^{-1}) and the exchange coupling constant associated with a fumarate bridge connecting equivalent Co(II) ions ($|J_{AA}^{1/2}| \approx 0.25$ (1) cm^{-1}), in good agreement with the average $J^{3/2}$ value determined from magnetic measurements.

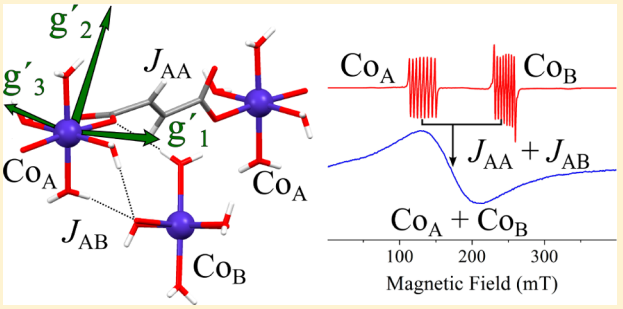

INTRODUCTION

The physicochemical characterization of high spin cobalt(II) coordination compounds is of interest because cobalt is present in several biological systems of central importance in nature and extensively used as a probe in cobalt-substituted zinc enzymes.[1−8] These compounds fulfill as well an essential role in industrial and technological applications as catalysts,[9−11] and in the design of materials with predetermined magnetic properties.[12−14] Considerable efforts have been devoted to understand the electronic properties of Co(II) ions using many spectroscopic techniques such as UV−vis, magnetic circular dichroism,[15,16] paramagnetic nuclear magnetic resonance,[8,17,18] electron paramagnetic resonance (EPR),[19−25] and electron−nuclear double resonance,[26,27] as well as magnetic techniques such as magnetic susceptibility and magnetization measurements.[28−30]

Magnetic studies of high spin Co(II) complexes provide information on both the electronic structure and the interactions between Co(II) ions. In the solid state, these studies are usually performed by using magnetic measurements and also, though less frequently, by EPR spectroscopy. While the former is used principally for evaluating the zero field splitting (ZFS) parameters (D and E) and exchange coupling constants among metal centers larger than 1 cm^{-1}, the latter is more appropriate to evaluate the tensorial magnitudes associated with anisotropic interactions and isotropic exchange coupling constants smaller than 1 cm^{-1}.[31,32] Particularly, when EPR spectroscopy is performed on oriented single crystals of pure metal complexes and on metal-doped diamagnetic hosts, it can be used to evaluate the orientation of the tensorial magnitudes relative to the molecular frame and the magnitudes of weak exchange interactions even in the presence of stronger interactions, and to learn how the different magnetic

Received: November 7, 2013
Published: February 14, 2014

   dx.doi.org/10.1021/ic402797t | *Inorg. Chem.* 2014, 53, 2535−2544

interactions between the metal centers modulate the EPR spectral properties of the isolated ions.[19,32−37] In summary, the information obtained from both EPR spectroscopy and magnetic measurements is very useful to fully understand the magnetic properties of a Co(II) system, although works exploiting these two techniques together are uncommon.

The free Co(II) ion in the high spin configuration ($S = 3/2$) presents a ^4F ground state, which in a pure octahedral field splits into two orbital triplets ($^4T_{1g}$ and $^4T_{2g}$) and one orbital singlet ($^4A_{2g}$), $^4T_{1g}$ being the ground-state multiplet. Additional distortions of the octahedral field split this ground level resulting in an orbital singlet ground state ($^4A_{2g}$) and an orbital doublet excited state (^4E_g). The components of the $^4A_{2g}$ state can be split into two doublets ($M_S = \pm 1/2$ and $M_S = \pm 3/2$), even in zero magnetic field, by spin−orbit coupling with excited states, with the energy separation between these two doublets being the ZFS. Despite that the two split doublets of the $^4A_{2g}$ cannot be considered pure in character, this nomenclature will be used throughout the text for simplicity. A common situation is that only the lowest Kramers doublet is thermally populated, as the EPR signals of Co(II) ions are detected usually at temperatures lower than 20 K due to the fast relaxation rate of this metal. Since this ground level is split into two components by the Zeeman interaction, it may be treated as an effective spin $S' = 1/2$ and hence the magnetic properties can be analyzed from a simple Zeeman Hamiltonian characterized by a $\mathbf{g}'$-tensor associated with the ground doublet. The determination of the eigenvalues and eigenvectors of the $\mathbf{g}'$-tensor is essential to understand the electronic properties of the metal centers and to establish correlations between magnetism and structure. However, as only a few works have been devoted to characterize the $\mathbf{g}'$-tensor and its correlation with structural properties of the Co(II) center, no clear correlation exists until now. The few single crystal EPR studies reported on high spin octahedral Co(II) compounds seem to indicate that small deviations from rigorous symmetry result in dramatic changes of the axial symmetry expected for the $\mathbf{g}'$-tensor.[19,38,39] Hence, to test this statement, we evaluated eigenvalues and eigenvectors of the $\mathbf{g}'$-tensor in a nearly octahedral high spin Co(II) site having ligands with similar strength, which constitutes one of the objects of this paper.

Interactions such as dipolar and exchange may produce both magnetic and spectroscopic behaviors different from those of the isolated ions. The exchange phenomenon is well understood both experimentally and theoretically for the simpler case of weakly, intermediate, and strong exchange coupled systems with $S = 1/2$.[32,33,40−44] However, exchange coupled systems with spins $S > 1/2$, which in addition present an unquenched orbital angular momentum as is the case of high spin Co(II) ions, are less studied. Again, as for the case of the $\mathbf{g}'$-tensor, one of the problems is the lack of enough experimental data that correlate the exchange coupling constant derived from magnetic measurements ($J^{3/2}$) with that derived from the EPR data considering a doublet $S' = 1/2$ ($J^{1/2}$). The $J^{3/2}$ and $J^{1/2}$ relation, which is usually omitted in most magnetic studies on high spin Co(II) compounds, has been earlier analyzed theoretically but only for cases in which the Zeeman term is the dominant.[45,46] In this work we use a more complete approach that contemplates the influence of the ZFS and the exchange interaction between $S = 3/2$ spins to the exchange interaction constants that couple the effective S' spins to correlate the exchange parameters obtained from both techniques with the different chemical pathways linking Co(II) ions, which constitutes the second object of the paper.

We present a detailed powder and single-crystal EPR study together with magnetic susceptibility and magnetization measurements of the coordination polymer *catena*-(*trans*-(μ_2-fumarato)tetraaquacobalt(II)) [$(C_4H_{10}CoO_8)_n$], and the Co(II)-doped Zn(II) analogue, hereafter **1** and **2**, respectively. The magnetic measurements of **1** revealed the presence of weak exchange interactions between the Co(II) ions of the crystal lattice, that could be selectively evaluated from single crystal EPR spectroscopy studies performed on **1** and **2**. The orientation of the $\mathbf{g}'$-tensor relative to the molecular frame is compared with results obtained for other Co(II) complexes. We also analyze the role of weak exchange interactions in modulating the transition between the uncoupled ↔ coupled high spin Co(II) ion regimes.

EXPERIMENTAL SECTION

Materials. All chemicals, of commercially available reagent grade, were used as received. Water was purified by a Millipore Milli-Q system, yielding 18 MΩ cm water.

1. The compound was prepared in a different way from that reported elsewhere.[47] $Co(NO_3)_2{\cdot}6H_2O$ (10 mmol, 2.91 g, Merck) and fumaric acid (10 mmol, 1.16 g, Sigma) were dissolved in 30 mL of water, the pH was adjusted to 3.5 with 0.1 M NaOH, and the solution was filtered using a 0.22 μm Millipore cellulose nitrate membrane and left to evaporate slowly at room temperature. After a few days rose-colored prismatic single crystals were obtained, which were filtered, washed with a small amount of cold water, and dried in air.

2. The crystal structure of the coordination polymer *catena*-(*trans*-(μ_2-fumarato)tetraaqua-Zn(II)) [$(C_4H_{10}ZnO_8)_n$], which is isostructural to **1**, was reported some years ago.[48] This compound was prepared as described for **1** replacing $Co(NO_3)_2{\cdot}6H_2O$ by $ZnSO_4{\cdot}7H_2O$ (10 mmol, 2.875 g, Mallinckrodt). Cobalt was added in a 1:10, 1:20, or 1:30 Co:Zn ratio. In few weeks slightly pink crystals grew in the solution. Powder samples were obtained by grinding single crystals. The structures of both compounds were confirmed by powder X-ray diffraction data obtained on a Shimadzu XD-D1 diffractometer and elemental analysis (Carlo Erba EA1108). The morphology of the single crystals, necessary to orient the sample for the EPR experiment, was determined by measuring the angles between crystal faces using a Carl Zeiss Axiolab goniometric microscope. Single crystals of **1** and **2** showed well developed (010) and (11$\bar{1}$) faces, respectively.

Magnetization and Magnetic Susceptibility Measurements. Magnetic data were obtained with a Quantum Design MPMS-XL5 SQUID magnetometer. Magnetization and magnetic susceptibility measurements were performed respectively on 61.25 mg of a powder sample of **1** encapsulated on a gelatin container of known diamagnetic contribution as a function of the external DC magnetic field (between 0 and 50 kOe) at $T = 2$ K and as a function of temperature (between 2 and 300 K) at 0.5 kOe. Diamagnetic (DIA) and temperature independent paramagnetism (TIP) contributions were estimated by fitting the 200−300 K range of the χT versus T curve with a straight line. The slope of this line corresponds to ($\chi_{DIA} + \chi_{TIP}$),[49] and this quantity was added to the simulated magnetization and magnetic susceptibility curves ($\chi_{DIA} + \chi_{TIP} = 740 \times 10^{-6}$ cm^3 mol^{-1}). The χ_{DIA} contribution using Pascal's constants was evaluated to be -110×10^{-6} cm^3 mol^{-1}, affording $\chi_{TIP} = 850 \times 10^{-6}$ cm^3 mol^{-1}, compatible with octahedral Co(II) complexes.[50]

EPR Measurements. X-band CW-EPR spectra of oriented single crystals and powdered samples of **1** and **2** were obtained at 5 K on a Bruker EMX-Plus spectrometer, equipped with an Oxford Instruments helium continuous-flow cryostat and a rectangular cavity with 100 kHz field modulation.

A single crystal of **1** was oriented by gluing its (010) face to a cleaved KCl cubic holder, which defined a set of orthogonal laboratory axes with the y direction corresponding to the crystal b axis, a fact confirmed by the symmetry of the angular variation of the EPR signals

dx.doi.org/10.1021/ic402797t | Inorg. Chem. 2014, 53, 2535−2544

in the *xy* and *zy* planes. The cubic sample holder was placed on the top of a Rexolite cylinder which was fitted to the end of a 4 mm OD quartz tube, as explained elsewhere.[34] The tube was positioned at the center of the microwave cavity and attached to a goniometer which allowed the sample to be rotated in 10° intervals with the magnetic field in the *xy*, *zx*, and *zy* ($y\|b$ and $x\|[101]$) planes of **1**. For **2**, a $(11\bar{1})$ face was glued to a Rexolite prismatic triangular sample holder (see Figure S1 in the Supporting Information), built with a 68.0° angle (the angle between the (010) and the $(11\bar{1})$ crystal planes). The sample holder was placed on top of the Rexolite cylinder, and the rest of the procedure was exactly the same as for the **1** crystal.

RESULTS AND DISCUSSION

Crystal and Molecular Structure. A brief description of the crystal structures of **1** and its Zn(II) analogue is presented in order to interpret the EPR experiment. **1** crystallizes in the monoclinic system $P2_1/c$, $Z = 4$.[47] Relevant crystal data are given in Table S1 in the Supporting Information. The Co(II) ions are in a slightly distorted octahedral environment coordinated to four water oxygen atoms and *trans* coordinated to two carboxylic oxygen atoms from the fumarate anions (Figure 1). The four symmetry related Co(II) ions of the unit cell are designated as A (x,y,z), A′ $(-x,-y,-z)$, B $(-x,1/2+y,1/2-z)$, and B′ $(x,1/2-y,1/2+z)$.

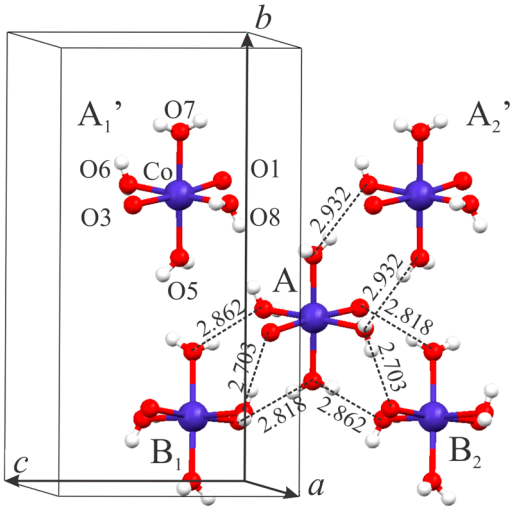

Figure 1. Perspective of the crystal unit cell showing the coordination around the Co(II) ions and hydrogen bonds between magnetically equivalent and inequivalent Co(II) ions. Labels and hydrogen bond distances in Å are also indicated.

Magnetically equivalent Co(II) ions of the same type (A(B), A′(B′)) are bridged by fumarate anions, which results in a polymeric −Co−fumarate−Co− chain (d_{Co-Co}, 9.819 Å) along the [101] direction (Figure 2). A(B) and A′(B′) chains are related by an inversion symmetry operation and therefore are magnetically equivalent, whereas A(A′) and B(B′) chains are related by the monoclinic C_2 rotation around the *b* axis, and hence magnetically inequivalent. The nearest Co−Co distances between Co(II) ions belonging to neighboring chains are indicated in Figure 2. This polymeric structure is stabilized through a network of hydrogen bond interactions that involve the cobalt ligands shown in Figure 1. There are three H-bonds connecting an A-type Co(II) ion with two B-type Co(II) ions identified as B_1 and B_2, and two H-bonds with an A′-type Co(II) ion identified as A_2' (for H-bond distances and angles

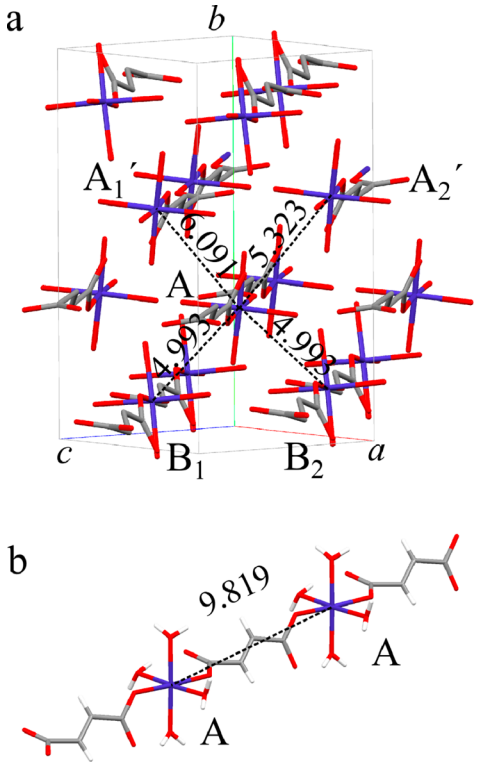

Figure 2. (a) Perspective of the crystal unit cell showing the Co−fumarate−Co chains along the [101] direction. The nearest Co−Co distances in Å between Co(II) ions belonging to neighboring chains are indicated. (b) A single Co−fumarate−Co chain with the Co−Co distance indicated in Å.

see Table S2 in the Supporting Information). There are no direct H-bonds between A and A_1' ions.

The coordination around the Zn(II) ion is very similar to that around the Co(II) ion, with slight differences in the metal−ligand bond distances. Crystal and molecular structure information for the Zn(II) compound is shown in Table S1 in the Supporting Information.

Magnetic Measurements. Temperature-dependent magnetic susceptibility (χ) and field-dependent magnetization (M) results are shown in Figure 3.

The data in Figure 3 were interpreted using a general model in which the magnetic properties were calculated from exact numerical diagonalization of an energy matrix derived from a spin Hamiltonian in the $S = 3/2$ basis. This spin Hamiltonian included the Zeeman interaction, axial (D) and rhombic (E) zero field splitting, and exchange interaction within a molecular field approximation,[50]

$$H = \mu_B \mathbf{S}\cdot\mathbf{g}\cdot\mathbf{H} + D\left(S_z^2 - \frac{S(S+1)}{3}\right) + E(S_x^2 - S_y^2) - zJ^{3/2}\langle S_z\rangle S_z \quad (1)$$

where all the symbols have their usual meaning in the study of bulk magnetic properties, and z corresponds to the number of first neighbors linked to each Co(II) ion by the chemical paths described in Figures 1 and 2 ($z = 5$). The principal axis of the **D**-tensor ($D = (3/2)D_Z$ and $E = (1/2)(D_X - D_Y)$) is used as the quantization axis.[51] In this reference frame, the **g**-tensor is not necessarily diagonal. However, as the ZFS term is larger than the Zeeman energy, the **g**-tensor can be assumed to be either isotropic or coaxial with the **D**-tensor.[52,53] The best

dx.doi.org/10.1021/ic402797t | Inorg. Chem. 2014, 53, 2535−2544

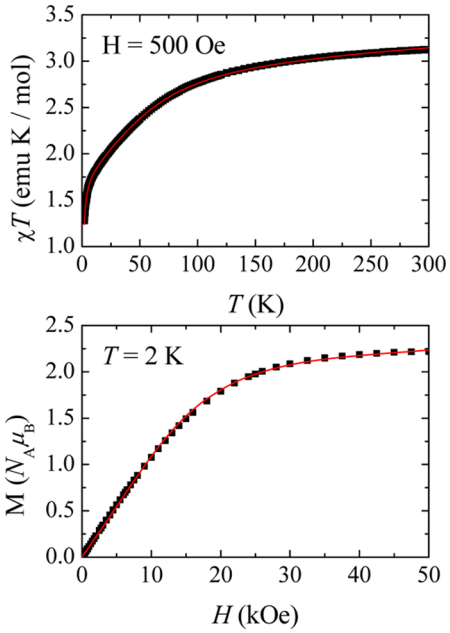

Figure 3. Temperature dependence of the χT (top) as a function of temperature at H = 0.5 kOe and molar magnetization M in $N_A\mu_B$ units as a function of magnetic field at T = 2 K (bottom) of a powder sample of **1**. The solid lines were obtained by least-squares fitting as explained in the text.

agreement with experiment was obtained assuming axial and isotropic **g**-tensors for the magnetization and susceptibility data, respectively (see Table 1). The **g**-tensor parameters and the E/D ratio used in the simulations were obtained from the EPR results presented below. Even initializing the calculation with positive values of $J^{3/2}$, the exchange interaction resulted to be always antiferromagnetic in nature. Although the D-values determined by both methods show some difference, they are within the expected ones for high spin Co(II) ions in octahedral coordination.[28] The difference observed is not uncommon for large D-values, where magnetization was shown to be more sensitive to determine ZFS parameters.[29]

Table 1. Best Fit Parameters of the Curves χT vs T and M vs H

data type	constrained parameters	optimized parameters	sum of squares of the deviations
χT vs T	$g_x = g_y = g_z = g_{iso}$ E/D = 0.016	g_{iso} = 2.515 D = 65 cm^{-1} $zJ^{3/2}$ = −0.47 cm^{-1}	0.0115
M vs H	$g_\perp$ = 2.50 $g_\parallel$ = 2.61 E/D = 0.016	D = 43 cm^{-1} $zJ^{3/2}$= −0.28 cm^{-1}	0.0094

Powder EPR Measurements. EPR spectra of powder **2** samples with different Co:Zn ratios are shown in Figure 4. The spectra are typical of a high spin (S = 3/2) Co(II) ion in octahedral coordination, in which only the ground doublet (M_S = ±1/2) is thermally populated.[19,23]

The diluted samples showed a nearly axial spectrum with resolved hyperfine structure with the cobalt nucleus (I = 7/2) at $g_\perp$. In contrast, **1** shows a unique broad resonance line with no resolved hyperfine structure. The higher the Co(II) ion concentration, the lower the hyperfine structure resolution,

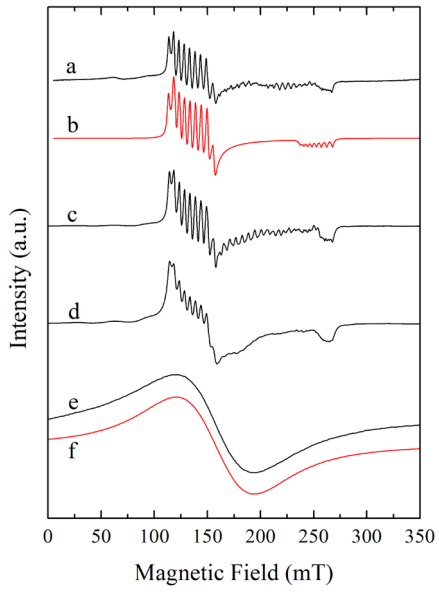

Figure 4. Powder EPR spectra of **2** in 1:30 (a), 1:20 (c), and 1:10 (d) Co:Zn ratios and pure **1** (e) taken at 9.4 GHz and 5 K under nonsaturating conditions, together with simulation of the 1:30 diluted (b) and pure (f) spectra.

which confirms that the collapse of the hyperfine structure in the pure sample is due to the presence of magnetic interactions between Co(II) ions, in line with the magnetic data that showed exchange-coupled Co(II) ions. It is important to note the presence of low intensity extra resonances between the $g_\perp$ and $g_\parallel$ features in spectrum a, which originate, as discussed below, from pairs of exchange-coupled Co(II) ions randomly substituting Zn(II) ions. The intensity of these satellite signals, which are also observed in the single crystal spectra of **2**, increases in the sample with 1:20 Co:Zn ratio (spectrum c), but cannot be discernible in the more concentrated samples because of broadening effects due to the higher number of interacting Co(II) ions.

Spectrum e was simulated using an effective Zeeman Hamiltonian with S' = 1/2, whereas spectrum a was simulated in a similar manner but including, in addition to the Zeeman term, the hyperfine interaction with the Co(II) nucleus (I = 7/2),

$$H = \mu_B \mathbf{S}'\cdot\mathbf{g}'\cdot\mathbf{B} + \mathbf{S}'\cdot\mathbf{A}\cdot\mathbf{I} \quad (2)$$

where all the symbols have the usual meaning in magnetic resonance. The eigenvalues and eigenvectors of the **g**′- and **A**-tensors used in the simulation were taken from the single-crystal EPR experiments performed on **1** and **2** described below (see Tables 2, 3, and 4). The **A**-tensor in eq 2 must be taken also as an effective tensorial magnitude, as represents the

Table 2. Components, Eigenvalues, and Eigenvectors of Crystal g′^{2}-Tensor for 1 in the Experimental *xyz* Coordinate System

g'^2_{xx} = 17.37(14)	g'^2_{xy} = 0.0(2)
g'^2_{yy} = 14.58(12)	g'^2_{zx} = 2.2(2)
g'^2_{zz} = 25.64(14)	g'^2_{zy} = 0.0(2)
g'_1 = 4.10(8)	$\mathbf{a}_1$ = [0.969(8), 0.02(9), −0.24(2)]
g'_2 = 3.81(6)	$\mathbf{a}_2$ = [0.01(9), −0.999(5), −0.00(2)]
g'_3 = 5.12(9)	$\mathbf{a}_3$ = [−0.24(2), −0.00(2), −0.969(5)]

dx.doi.org/10.1021/ic402797t | Inorg. Chem. 2014, 53, 2535−2544

Table 3. Components of the Molecular g'^2-Tensor and Eigenvalues and Eigenvectors of the g'-Tensor Associated with the Co(II) Ions in 2 in the Experimental *xyz* Coordinate System[a]

g'^2_{xx} = 17.46(4)		g'^2_{xy} = ∓ 9.60(4)
g'^2_{yy} = 16.17(4)		g'^2_{zx} = 1.63(6)
g'^2_{zz} = 23.56(5)		g'^2_{zy} = ± 1.90(6)
g'_1 = 4.89(2)	$\mathbf{a}_1$ = [±0.13, 0.08, ± 0.988]	$g_\parallel$ = 2.61
g'_2 = 5.14(2)	$\mathbf{a}_2$ = [±0.726, −0.686, ∓0.04]	$g_\perp$ = 2.50
g'_3 = 2.61(2)	$\mathbf{a}_3$ = [±0.675, 0.723, ∓0.148]	E/D = 0.016

[a]The upper (assignment I) and lower (assignment II) signs in the eigenvectors correspond to the two possible orientations of the $\mathbf{g}'$-tensor relative to the molecular frame. The spin Hamiltonian parameters ($g_\parallel$, $g_\perp$, and E/D) in the S = 3/2 base are also shown.

Table 4. Components, Eigenvalues, and Eigenvectors of the Molecular A-Tensor (in MHz) Associated with the Co(II) Ions in 2 in the Experimental *xyz* Coordinate System[a]

A_{xx} = 229(17)	A_{xy} = ∓126(10)
A_{yy} = 237(18)	A_{zx} = 5.9(4)
A_{zz} = 365(28)	A_{zy} = ±18(1)
A_1 = 353(27)	$\mathbf{a}_1$ = [±0.6015, −0.5654, ±0.5644]
A_2 = 373(28)	$\mathbf{a}_2$ = [±0.3562, −0.4425, ∓0.8230]
A_3 = 105(8)	$\mathbf{a}_3$ = [±0.7151, 0.6960, ∓0.0648]
$\angle A_3$–g_3 = 5.5°	$\angle A_1$–g_1 = 54.1°
$\angle A_1$–g_2 = 36.36°	$\angle A_2$–g_2 = 53.8°
$\angle A_2$–g_1 = 36.4°	

[a]The upper (assignment I) and lower (assignment II) signs in the eigenvectors correspond to the two possible orientations of the **A**-tensor relative to the molecular frame. The angles between the eigenvectors of the **A**- and $\mathbf{g}'$-tensors are also given.

interaction of the fictitious S' = 1/2 of the Co(II) ions with the true nuclear spin of the cobalt nucleus. For spectrum a, the presence of interacting Co(II) ions was not considered in the simulation (spectrum b).

Single Crystal EPR Measurements. For a monoclinic system consisting of an extended lattice of noninteracting Co(II) ions, one would expect, under the experimental conditions of the EPR assay, one group of eight hyperfine components for any magnetic field orientation in the *ca* plane and along the *b* axis, and two groups for any other direction. This situation was clearly observed in the angular variation of the single crystal EPR spectra of **2** (Figure 5; the full angular variation of the spectra is shown as Supporting Information in Figure S2). In contrast, EPR spectra of **1** showed only one broad resonance line with linewidths in the 40–90 mT range for any magnetic field orientation (Figure 5, the full angular variation of the spectra is shown as Supporting Information, Figure S3).

The single resonance line observed in **1** (Figure 5) can be produced by interactions such as dipolar coupling, and anisotropic and antisymmetric exchange between Co(II) ions which broaden the individual resonance lines, and isotropic exchange that causes narrowing rather than broadening.[31] The single line obtained along the *x*-axis shows a breadth of the order of the hyperfine pattern, indicating that exchange interactions between either A–A (B–B) Co(II) ions ($J^{1/2}_{AA} = J^{1/2}_{BB}$) or A–B Co(II) ions ($J^{1/2}_{AB}$) are strong enough to merge the hyperfine structure; the two groups of eight hyperfine lines are merged to a single line with a position corresponding to the average of the g'^2-factors of the A and B sites, indicating that $z|J^{1/2}_{AB}| \geq \mu_B \Delta g B/2$. These two results together allowed us to estimate $|J^{1/2}_{AB}| \approx 0.055(2)$ cm^{-1} (z = 2 corresponds to the number of inequivalent first neighbors linked to each Co(II), see Figure 1), i.e., a $J^{1/2}_{AB}$-value of the order of the Zeeman energy difference between inequivalent Co(II) ions.[33,41]

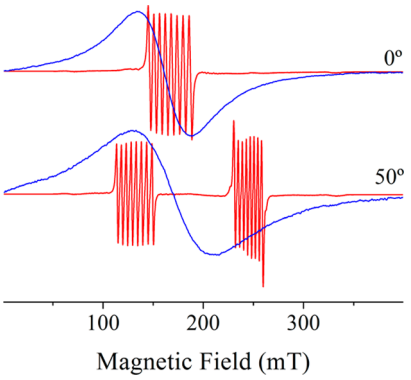

Figure 5. Representative single crystal EPR spectra of **1** (blue) and **2** (red) for two magnetic field orientations in the *xy* plane. The central positions of the spectra for the diluted and pure compounds do not match exactly due to a slight different alignment of the single crystal inside the EPR cavity and also to a little difference between the $\mathbf{g}'$-tensors (see Tables 2 and 3). Upper and lower spectra were taken with the magnetic field at 0° and 50° from the *x*-axis, respectively.

Crystal $\mathbf{g}'$-Tensor. In many of the EPR spectra of **1** (Figure S3 in Supporting Information) the single resonance lines are asymmetrical. This phenomenon occurs at low magnetic fields of the EPR experiment when the magnetic field of the maximum absorption is of the same magnitude as the line width.[54] This asymmetry can be explained taking into account that the linearly polarized microwave field that induces the transitions between two spin states in a typical continuous wave EPR experiment can be decomposed into two circularly polarized components (right and left circularly polarized microwave fields). The right circularly polarized microwave induces an EPR transition at $+B_0$ (positive magnetic field axis) whereas the left circularly polarized microwave induces one at $-B_0$ (negative magnetic field axis). When the line width is lower than the magnetic field position of the resonance line, these two resonances do not overlap. In contrast, when the line width is comparable in magnitude with the position of the resonance line, as is the case of high spin Co(II) ions, part of the resonance line at $-B_0$ can fall on the positive magnetic field axis, and vice versa, yielding a partial overlap of the resonances at $+B_0$ and $-B_0$ that causes an asymmetry in the resonance line shape (see Figure S4 in the Supporting Information). Therefore, the spectra of **1** were fitted with the sum of two Lorentzian derivative functions centered at $+B_0$ and $-B_0$ with the same intensity and line width. The $+B_0$ values of the spectra were used to calculate the angular variation of g'^2-factors shown in Figure 6. The components of the crystal $\mathbf{g}'^2$-tensor were obtained by least-squares fitting eq 3 to the data and are given in Table 2 together with its eigenvalues an eigenvectors.

$$g'^2(\theta, \varphi) = g'^2_{xx} \sin^2\theta \cos^2\varphi + g'^2_{yy} \sin^2\theta \sin^2\varphi + g'^2_{zz} \cos^2\theta + 2g'^2_{xy} \sin^2\theta \cos\varphi \sin\varphi + 2g'^2_{zx} \sin\theta \cos\varphi \cos\theta + 2g'^2_{zy} \sin\theta \sin\varphi \cos\theta \quad (3)$$

dx.doi.org/10.1021/ic402797t | Inorg. Chem. 2014, 53, 2535–2544

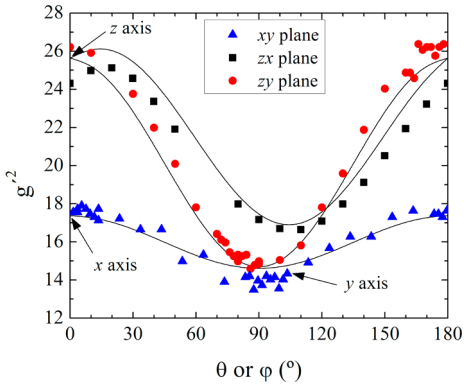

Figure 6. Angular variation of $g'^2(\theta,\varphi)$ in three planes of **1**. The data correspond to the crystal $\mathbf{g}'$-tensor, $\mathbf{g}'^2 = (\mathbf{g}_A'^2 + \mathbf{g}_B'^2)/2$. The *x*, *y*, and *z* directions of the reference system are indicated on the figure.

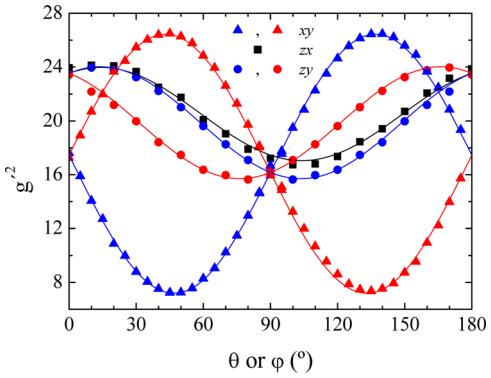

Figure 7. Angular variation of $g'^2(\theta,\varphi)$ for the two magnetically inequivalent Co sites in three planes of **2**. The colors red and blue indentify the two inequivalent Co(II) ions of the unit cell. Only one line is observed in the *zx* plane because the two Co(II) ions are magnetically equivalent in that plane.

The solid lines in Figure 6, obtained using the g'-values of Table 2 and eq 3, are in good agreement with experiment. The differences observed for some orientations are attributed to the uncertainties in the fitting of the line positions which arise from the asymmetry and the large width of the resonances and some misalignment of the single crystals produced during the successive remounting of the single crystal inside the EPR cavity. It is worth noting that the crystal $\mathbf{g}'^2$-tensor evaluated by the single crystal EPR experiment does not allow us to determine the molecular $\mathbf{g}'$-tensor corresponding to single Co(II) ions, as the individual resonances are collapsed by exchange interactions. The molecular $\mathbf{g}'$-tensor associated with the Co(II) site could be determined from single-crystal EPR experiment performed on **2**, as explained below.

Molecular g′- and A-Tensor. The single crystal EPR spectra of **2** (Figure S2 in Supporting Information) were analyzed using eq 2 taking into account that there are two magnetically inequivalent Co(II) ions in the unit cell. The central position B_0 and the separation a between the lines of each octet were determined by using a program developed in Matlab. This program differentiates every spectrum to obtain the second-derivative of the EPR signals, in which the minima correspond to the position of each resonance line. These positions were automatically located using a local minima search routine with appropriate criteria to minimize noise effects.

The central positions B_{0A} and B_{0B} were used to evaluate the $\mathbf{g}_A'^2$- and $\mathbf{g}_B'^2$-tensors in the *xyz* coordinate system (Figure 7) by least-squares fitting eq 3 to the experimental values. As seen in Figure 7, this experiment allows differentiating the angular variation of the g'-factors associated with the two inequivalent A and B Co(II) sites, which are equivalent only in the *zx* plane.

The eigenvalues and eigenvectors of the molecular $\mathbf{g}'$-tensors in the *xyz* axes system are given in Table 3 and were used to obtain the solid lines in Figure 7. The table also shows the parameters $g_\perp$, $g_\parallel$, and E/D assuming an axial **g**-tensor coaxial with the **D**-tensor. These parameters, which were derived from the eigenvalues of the $\mathbf{g}'$-tensor,[55,56] were used to fit both the magnetization and susceptibility data, as explained above. The $g_\perp$ and $g_\parallel$ values lie in the range of 2.1−2.8 reported for high spin Co(II) ions in octahedral coordination.[57] The experimental isotropic g'-value (g = 4.37) is in good agreement with the g'-value of ∼4.3 evaluated solely from theoretical considerations for sites of strict octahedral symmetry. The anisotropy of the $\mathbf{g}'$-tensor displayed by **1** is within the typical values reported for high spin Co(II) ions in octahedral coordination with small distortions.[45,58]

The effective hyperfine **A**-tensor was obtained from the eigenvalues to first order of the spin Hamiltonian given in eq 2 using[51]

$$K^2(\theta,\varphi) = \frac{\mathbf{h}\cdot\mathbf{g}'\cdot\mathbf{A}\cdot\mathbf{A}\cdot\mathbf{g}'\cdot\mathbf{h}}{g'^2(\theta,\varphi)} \quad (4)$$

where $K = ag'\mu_B$, and $\mathbf{h} = [\sin\theta\cos\varphi; \sin\theta\sin\varphi; \cos\theta]$ is the unit vector along the magnetic field **B** in the *xyz* system. Figure 8 shows the angular variation of K^2 for the A and B sites in three crystal planes of **2**. The symbols and the colors have the same meaning as in Figure 7.

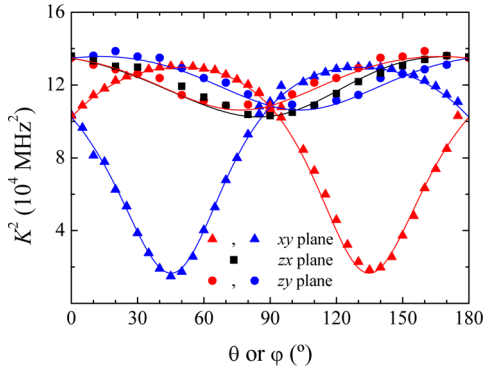

Figure 8. Angular variation of $K^2(\theta,\varphi)$ for the A and B Co(II) ions in three crystal planes of **2**. The symbols and the colors have the same meaning as in Figure 7.

The eigenvalues and eigenvectors of the molecular **A**-tensors in the *xyz* axis system are shown in Table 4 and were used to obtain the solid lines in Figure 8.

The results presented in Tables 3 and 4 show that the $\mathbf{g}'$- and **A**-tensors are nearly axial, with g_3' and A_3 eigenvectors nearly coincident ($\angle A_3 - g_3' = 5.5°$). The remaining $\mathbf{g}'$- and **A**-tensor eigenvectors are almost in the same plane but are not coincident ($\angle A_1 - g_1 = 54.1°$).

Because of the monoclinic symmetry of the crystal lattice of **1**, there are two possible orientations for the molecular $\mathbf{g}'$-tensor, which are indicated in Table 3. The symmetry of the

dx.doi.org/10.1021/ic402797t | Inorg. Chem. 2014, 53, 2535−2544

molecular **g**′-tensor must follow the symmetry of the metal site. For instance, for metal sites with strict axial symmetry (e.g., molecules belonging to point group D_{4h}), the eigenvector associated with $g'_{\parallel}$ must lie on the axial axis (the molecular z axis), whereas the remaining two eigenvectors associated with the two $g'_{\perp}$ eigenvalues must lie on the equatorial ligand plane. For metal sites with lower symmetry but still presenting an axial distortion, e.g., D_{2h}, the $g'_{\perp}$ eigenvectors must lie also on the equatorial ligand plane but pointing either along the bonds or between the bonds. Departures from these idealized geometries are found in most paramagnetic systems, which is reflected in their EPR properties with different extent. However, when this departure is not considerable, the **g**-tensor may follow the approximate symmetry around the metal site, which results in nearly axial **g**-tensors with eigenvectors lying approximately along molecular directions close to the true axes in an idealized symmetry. These particular molecular directions are usually identified as molecular pseudosymmetry axes. Representative examples of systems with these characteristic are Cu(II) complexes in nearly square planar coordination where the eigenvectors are lying approximately along pseudosymmetry axes of the metal site.[23,33,36]

The near axiality of the molecular **g**′-tensor associated with the Co(II) ions of **1** would suggest that its eigenvectors should lie along characteristic molecular directions (e.g., metal−ligand bonds). This situation was observed in distorted octahedral Co(II) compounds in which the g'_z eigenvector (g'_3 in our nomenclature) was found to be lying nearly along the axial direction of the Co site.[38,39] By contrast, we found that the g'_z = 2.23 component in a *trans*-N_2-*cis*-O_2(carboxylato)-*cis*-O_2(aquo)-type distorted octahedral cobalt(II) site is lying along a direction bisecting Co−O_c and Co−O_w bonds (O_c and O_w being carboxylic and water oxygen atoms, respectively) perpendicular to the longest ligand bond with the weaker N-ligand.[19] Figure 9 shows one possible orientation of the **g**′-tensor relative to the molecular frame in **1**, whereas the second possibility is shown in Figure S5 as Supporting Information. In principle, there is no immediate reason to choose one assignment over the other, since the smallest eigenvalue of the **g**′-tensor for both possibilities is not lying along any preferential bond direction. The data reveal that g'_3 is close to the $O_3O_5O_7O_1$ plane forming a 33° angle with the O_7CoO_5 direction for assignment I (Figure 9). A similar conclusion can be obtained for assignment II (Figure S5 in the Supporting Information), but in this case with larger deviation. This result together with that of ref 19 seems to indicate that the g'_3 eigenvector does not necessarily lie nearly along the tetragonal distortion axis. In summary, in Co(II) compounds having roughly octahedral geometry with the same type of ligands and presenting nearly axial EPR spectra, the presence of molecular pseudosymmetry axes in the metal site does not seem to determine preferential directions for the molecular **g**′-tensor.

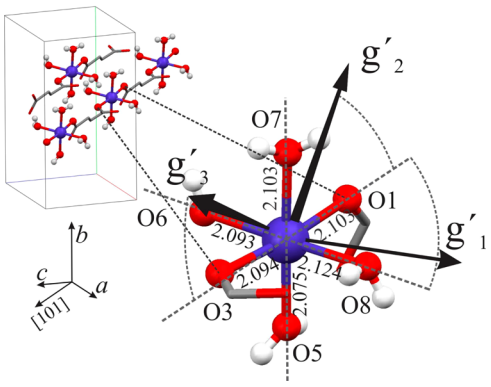

Figure 9. Assignment I for the orientation of the molecular **g**′-tensor in the molecular frame. The g'_3 eigenvector is approximately contained in the $O_3O_5O_7O_1$ plane, forming a 33° angle with the O_7−Co−O_5 direction, while the g'_1 eigenvector forms an angle of 12° with the O_6−Co−O_8 direction.

Exchange Interactions between Co(II) Ions. The magnetization and magnetic susceptibility results (see Figure 3 and Table 1) showed that there are small antiferromagnetic interactions between the S = 3/2 spin Co(II) ions, which could be accounted for in average, without discriminating between A−A (B−B) and A−B type exchange interactions. The single crystal EPR experiment on both **1** and **2** allowed us instead to estimate specifically $|J_{AB}^{1/2}| \approx 0.055$ cm^{-1} (see Figure 5). Additional information can be obtained from the analyses of the low intensity features detected in the single crystal EPR spectra of **2** (Figure 10). As shown in this figure, in addition to the eight resonance lines associated with isolated S' = 1/2 Co(II) ions, low intensity satellite lines are observed at both sides of the octets. These satellite lines can be associated mainly with the formation of statistically allowed pairs of interacting Co(II) ions. As described in Crystal and Molecular Structure (see Figures 1 and 2), each A-type Co(II) ion has two magnetic neighbors of the same type bridged by fumarate ions, two of B-type bridged by H-bonds, and one of A′-type also bridged by H-bonds. For symmetry reasons, the same situation occurs for the other Co(II) ions in the unit cell. For a Co:Zn ratio of about 1:30, the occupation probability $P = P_A + P_{A'} + P_B + P_{B'}$ for mononuclear Co(II) ion substitution is 1:30 for mononuclear and 1:900 for the possible dinuclear species. This determines the coexistence of mononuclear−dinuclear species contributing to the EPR spectrum with an intensity ratio of $n/z \times$ 1:30, n being the number of possible dinuclear species linked by a given chemical path (n = 2 for A−A, n = 2 for A−B, and n = 1 for A−A′ pairs). Within the experimental error, this ratio is detected in the experiment despite the low resolution of the dimeric EPR signal (see Figure 10).

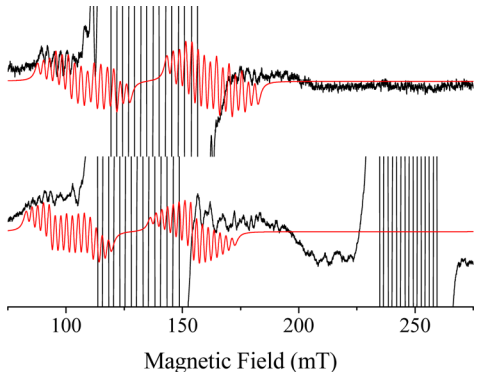

Figure 10. Single-crystal EPR spectra of **2** for two different magnetic field orientations (black), along the z axis (top) and at 50° from the x axis in the xy plane (bottom) together with simulations (red) . The ordinate scale is increased to show more clearly the weak satellite resonance lines.

The spin Hamiltonian for a pair of interacting S' = 1/2 Co(II) ions can be written as

dx.doi.org/10.1021/ic402797t | Inorg. Chem. 2014, 53, 2535−2544

$$H = \mu_B(\mathbf{S}'_i\cdot\mathbf{g}'_i + \mathbf{S}'_j\cdot\mathbf{g}'_j)\cdot\mathbf{B} + \mathbf{S}'_i\cdot\mathbf{A}_i\cdot\mathbf{I}_i + \mathbf{S}'_j\cdot\mathbf{A}_j\cdot\mathbf{I}_j + \mathbf{S}'_i\cdot\mathbf{J}_{ij}^{1/2}\cdot\mathbf{S}'_j \quad (5)$$

where the sum over all the unit cells of the crystal is omitted for simplicity, i,j = A or B, and $\mathbf{J}_{ij}^{1/2}$ is a second order tensor that takes into account isotropic ($J^{1/2}$), anisotropic ($\mathbf{J}_{ani}^{1/2}$), and antisymmetric exchange interactions. The relationship between the $\mathbf{J}_{ij}^{1/2}$-tensor and the isotropic exchange interaction $J^{3/2}$ can be derived by comparing the energy matrix obtained from two $S = 3/2$ Co(II) ions coupled by isotropic exchange ($J^{3/2}$), with the one resulting from the coupling between two $S' = 1/2$ Co(II) ions coupled by $\mathbf{J}_{ij}^{3/2}$. This procedure, which is detailed in an appendix in the Supporting Information, yielded for magnetically equivalent Co(II) ions

$$J^{1/2} = 3J^{3/2}$$
$$J_{ani,z}^{1/2} = -2J^{3/2}$$
$$J_{ani,y}^{1/2} = J_{ani,x}^{1/2} = J^{3/2} \quad (6)$$

relations that are only applicable for the case of large axial ZFS, which is valid in **2** due to the low $E/D = 0.016$ ratio.

For two interacting $S' = 1/2$ Co(II) ions with identical $\mathbf{g}'$- and $\mathbf{A}$-tensors, as is the case of A−A and B−B dimers, eq 5 predicts in a first order approximation two multiplets of 15 lines separated by $\Delta = \{(3/2)(\mathbf{h}\cdot\mathbf{g}'\cdot\mathbf{J}_{ani}^{1/2}\cdot\mathbf{g}'\cdot\mathbf{h})/[g'^2(\theta,\varphi)]\}/[\mu_B g'(\theta,\varphi)]$, in which the lines within each multiplet are separated by $A/2$. For the A−B dimer, the satellite pattern should be more complex than for the A−A dimer, as the interacting centers present different g'- and A-values, except in the zx plane where the ions are magnetically equivalent. In this case, eq 5 predicts for the A−B dimer a spectrum with gravity center at $\sim g'^2 = (g_A'^2 + g_B'^2)/2$ consisting of four multiplets of 15 lines each showing different hyperfine spacing. Spectra with these features were not detected in the experiment, suggesting that the satellite lines are associated with A−A (B−B) dimers. Satisfactory simulations of the satellite line patterns in the zx plane and the outer ones of the two octects in the xy plane could be obtained using the $\mathbf{g}'$- and $\mathbf{A}$-tensors for the A−A dimers and a $\mathbf{J}_{ani}^{1/2}$-tensor coaxial to $\mathbf{g}'$ with components $|\mathbf{J}_{ani,z}^{1/2}| = 0.166(8)$ cm^{-1}, $\mathbf{J}_{ani,x}^{1/2} = \mathbf{J}_{ani,y}^{1/2} = \mathbf{J}_{ani,z}^{1/2}/2$, (red lines in Figure 10).

The information provided by EPR, which is based on exchange interactions between effective $S' = 1/2$ spins, is different from that obtained from magnetic measurements, which provides exchange parameters between $S = 3/2$ spins. Although the magnetic measurements cannot discriminate and hence evaluate selectively the exchange constants associated with the different chemical paths, the $\mathbf{J}_{ani,z}^{1/2}$ exchange parameters determined by EPR and eqs 6 predict $|J_{AA}^{3/2}| = 0.083(4)$ cm^{-1} ($|J_{AA}^{1/2}| = 0.25(1)$ cm^{-1}), in good agreement with the $zJ^{3/2}$ values ($z = 5$ is the number of neighbors connected to each Co(II) ion, see Figures 1 and 2b) determined from magnetic measurements (see Table 1). The exchange constant $|J_{AB}{}^{1/2}| \approx 0.055$ cm^{-1} is related to the hydrogen bond bridge path, as this is the unique chemical path that connects inequivalent Co(II) ions. In contrast, there are two possible assignments for $J_{AA}{}^{1/2}$, a fumarate molecule or a hydrogen bond bridge (Figures 1 and 2). We assign $|J_{AA}^{1/2}| = 0.25$ cm^{-1} to the fumarate bridge due to the larger donor−acceptor distances of the hydrogen bonds for the A−A dimer relative to that for A−B dimer (see Table S2 in the Supporting Information), which suggests that $J_{AA}^{1/2}$ mediated by hydrogen bond is smaller than $J_{AB}^{1/2}$.

The exchange constants reported here are in good agreement with exchange interaction parameters transmitted by chemical paths with similar topologies reported for other octahedral high spin Co(II) compounds. Rizzi et al. evaluated $|J^{1/2}| \approx 0.07$ cm^{-1} for a chemical path consisting of Co−O−H···O−Co.[19] Zhang et al. evaluated by magnetic measurements $J^{3/2} = -0.44$ cm^{-1} for the exchange interaction mediated by a fumarate molecule in the catenary compound $[Co(II)(\mu\text{-fumarato})(4\text{-methylpyridine})_2(H_2O)_2]_{\infty}$,[59] larger than $|J_{AA}^{3/2}| = 0.083$ cm^{-1} evaluated by us by EPR.

CONCLUSION

The present paper demonstrates that the unresolved EPR spectrum of high spin Co(II) ions in **1** is due to the presence of weak magnetic interactions that average the individual tensorial magnitudes associated with the Co(II) ions. Both magnetic and single crystal EPR measurements were employed to evaluate the $\mathbf{g}'$-tensor and the exchange interactions coupling the high spin Co(II) ions in **1**. Despite that the coordination around Co(II) ion is nearly octahedral and the $\mathbf{g}'$-tensor is nearly axial, none of its eigenvectors are lying either along or between the cobalt−ligand bonds, as expected for a metal complex in octahedral coordination. This result indicates that the principal directions of nearly axial $\mathbf{g}'$-tensors in high spin Co(II) sites cannot be used to predict the coordination geometry around the metal ion and vice versa, as occurs in the well-known case of $S = 1/2$ Cu(II) ion metal ions, where the $\mathbf{g}$-tensor eigenvectors are lying approximately along the pseudosymmetry axis of the molecule.

We have also been able to determine selectively exchange coupling constants that couple the Co(II) ions in **1**. Since the exchange constants determined by magnetic measurements and EPR spectroscopy use the spin basis $S = 3/2$ and $S' = 1/2$, respectively, we developed theoretical work to correlate the information obtained from these two different methodologies. The relations obtained correlate the values of the isotropic exchange coupling constant $J^{3/2}$ between $S = 3/2$ spins and both isotropic $J^{1/2}$ and anisotropic exchange $\mathbf{J}_{ani}^{1/2}$ constants that couple the $S' = 1/2$ spins. The exchange coupling constants determined with both methods reveal that the hydrogen bonds and the fumarate σ-skeleton connecting the Co(II) ions can transmit weak but non-negligible exchange interactions, strong enough to modify the magnetic behavior of the individual Co(II) ions.

These results reveal the selectivity and accuracy of single crystal EPR spectroscopy relative to magnetic techniques such as magnetic susceptibility and magnetization measurements, which can only determine an average value of the exchange coupling constants.

ASSOCIATED CONTENT

Supporting Information

Figures including the mounting of a single crystal of **2** for the EPR experiment, angular variation of the single crystal EPR spectra obtained in three planes of **1** and **2**, composition of two resonance lines centered at $+B_0$ and $-B_0$, assignment II for the orientation of the molecular $\mathbf{g}'$-tensor in the molecular frame, tables showing relevant crystal information for **1** and **2**, and an appendix with theoretical demonstration of the relation between $J^{3/2}$ and $\mathbf{J}_{ij}^{1/2}$-tensors. This material is available free of charge via the Internet at http://pubs.acs.org.

dx.doi.org/10.1021/ic402797t | Inorg. Chem. 2014, 53, 2535−2544

AUTHOR INFORMATION

Corresponding Author

*E-mail: brondino@fbcb.unl.edu.ar. Fax: + 54 342 4575221. Tel: + 54 342 4575213.

Notes

The authors declare no competing financial interest.

ACKNOWLEDGMENTS

We thank FONCyT, CONICET, and CAI+D-UNL for financial support. N.I.N. thanks CONICET for a fellowship grant. E.W. and C.D.B. are members of CONICET-Argentina.

REFERENCES

(1) Gavel, O. Y.; Bursakov, S. A.; Rocco, G. D.; Trincão, J.; Pickering, I. J.; George, G. N.; Calvete, J. J.; Shnyrov, V. L.; Brondino, C. D.; Pereira, A. S.; Lampreia, J.; Tavares, P.; Moura, J. J. G.; Moura, I. *J. Inorg. Biochem.* **2008**, *102*, 1380−1395.

(2) Gavel, O. Y.; Bursakov, S. A.; Calvete, J. J.; George, G. N.; Moura, J. J. G.; Moura, I. *Biochemistry* **1998**, *37*, 16225−16232.

(3) Roderick, S. L.; Matthews, B. W. *Biochemistry* **1993**, *32*, 3907−3912.

(4) Bennett, B. EPR of Cobalt-Substituted Zinc Enzymes. In *Metals in Biology: Applications of High-Resolution EPR to Metalloenzymes*, Hanson, G., Berliner, L., Eds.; Springer: New York, 2010; pp 345−370.

(5) Bennett, B.; Holz, R. C. *J. Am. Chem. Soc.* **1997**, *119*, 1923−1933.

(6) Hawk, M. J.; Breece, R. M.; Hajdin, C. E.; Bender, K. M.; Hu, Z.; Costello, A. L.; Bennett, B.; Tierney, D. L.; Crowder, M. W. *J. Am. Chem. Soc.* **2009**, *131*, 10753−10762.

(7) Griffin, D. H.; Richmond, T. K.; Sanchez, C.; Moller, A. J.; Breece, R. M.; Tierney, D. L.; Bennett, B.; Crowder, M. W. *Biochemistry* **2011**, *50*, 9125−9134.

(8) Llarrull, L. I.; Tioni, M. F.; Kowalski, J.; Bennett, B.; Vila, A. J. *J. Biol. Chem.* **2007**, *282*, 30586−30595.

(9) Ittel, S. D.; Johnson, L. K.; Brookhart, M. *Chem. Rev.* **2000**, *100*, 1169−1204.

(10) Britovsek, G. J.; Gibson, V. C.; Wass, D. F. *Angew. Chem., Int. Ed.* **1999**, *38*, 428−447.

(11) Gibson, V. C.; Spitzmesser, S. K. *Chem. Rev.* **2002**, *103*, 283−316.

(12) Alborés, P.; Rentschler, E. *Angew. Chem., Int. Ed.* **2009**, *48*, 9366−9370.

(13) Murrie, M. *Chem. Soc. Rev.* **2010**, *39*, 1986−1995.

(14) Lazzarini, I. C.; Carrella, L.; Rentschler, E.; Alborés, P. *Polyhedron* **2012**, *31*, 779−788.

(15) Larrabee, J. A.; Alessi, C. M.; Asiedu, E. T.; Cook, J. O.; Hoerning, K. R.; Klingler, L. J.; Okin, G. S.; Santee, S. G.; Volkert, T. L. *J. Am. Chem. Soc.* **1997**, *119*, 4182−4196.

(16) Daumann, L. J.; Comba, P.; Larrabee, J. A.; Schenk, G.; Stranger, R.; Cavigliasso, G.; Gahan, L. R. *Inorg. Chem.* **2013**, *52*, 2029−2043.

(17) Periyannan, G. R.; Costello, A. L.; Tierney, D. L.; Yang, K.-W.; Bennett, B.; Crowder, M. W. *Biochemistry* **2005**, *45*, 1313−1320.

(18) Tierney, D. L.; Gassner, G. T.; Luchinat, C.; Bertini, I.; Ballou, D. P.; Penner-Hahn, J. E. *Biochemistry* **1999**, *38*, 11051−11061.

(19) Rizzi, A. C.; Brondino, C. D.; Calvo, R.; Baggio, R.; Garland, M. T.; Rapp, R. E. *Inorg. Chem.* **2003**, *42*, 4409−4416.

(20) Jacobsen, F. E.; Breece, R. M.; Myers, W. K.; Tierney, D. L.; Cohen, S. M. *Inorg. Chem.* **2006**, *45*, 7306−7315.

(21) Ozarowski, A.; Zvyagin, S. A.; Reiff, W. M.; Telser, J.; Brunel, L.-C.; Krzystek, J. *J. Am. Chem. Soc.* **2004**, *126*, 6574−6575.

(22) Goñi, A.; Lezama, L.; Rojo, T.; Foglio, M.; Valdivia, J.; Barberis, G. *Phys. Rev. B* **1998**, *57*, 246−251.

(23) Tamayo, A.; Casabó, J.; Escriche, L.; González, P.; Lodeiro, C.; Rizzi, A. C.; Brondino, C. D.; Passeggi, M. C. G.; Kivekäs, R.; Sillanpää, R. *Inorg. Chem.* **2007**, *46*, 5665−5672.

(24) Rosa, V.; Gonzalez, P. J.; Avilés, T.; Gomes, P. T.; Welter, R.; Rizzi, A. C.; Passeggi, M. C.; Brondino, C. D. *Eur. J. Inorg. Chem.* **2006**, 4761−4769.

(25) Núñez, C.; Bastida, R.; Macías, A.; Valencia, L.; Neuman, N. I.; Rizzi, A. C.; Brondino, C. D.; González, P. J.; Capelo, J. L.; Lodeiro, C. *Dalton Trans.* **2010**, *39*, 11654−11663.

(26) Walsby, C. J.; Krepkiy, D.; Petering, D. H.; Hoffman, B. M. *J. Am. Chem. Soc.* **2003**, *125*, 7502−7503.

(27) Myers, W. K.; Scholes, C. P.; Tierney, D. L. *J. Am. Chem. Soc.* **2009**, *131*, 10421−10429.

(28) Ostrovsky, S.; Tomkowicz, Z.; Haase, W. *Coord. Chem. Rev.* **2009**, *253*, 2363−2375.

(29) Titiš, J.; Boča, R. *Inorg. Chem.* **2011**, *50*, 11838−11845.

(30) Lloret, F.; Julve, M.; Cano, J.; Ruiz-García, R.; Pardo, E. *Inorg. Chim. Acta* **2008**, *361*, 3432−3445.

(31) Calvo, R. *Appl. Magn. Reson.* **2007**, *31*, 271−299.

(32) Neuman, N. I.; Perec, M.; González, P. J.; Passeggi, M. C. G.; Rizzi, A. C.; Brondino, C. D. *J. Phys. Chem. A* **2010**, *114*, 13069−13075.

(33) Neuman, N. I.; Franco, V. G.; Ferroni, F. M.; Baggio, R.; Passeggi, M. C. G.; Rizzi, A. C.; Brondino, C. D. *J. Phys. Chem. A* **2012**, *116*, 12314−12320.

(34) Schveigkardt, J. M.; Rizzi, A. C.; Piro, O. E.; Castellano, E. E.; De Santana, R. C.; Calvo, R.; Brondino, C. D. *Eur. J. Inorg. Chem.* **2002**, 2913−2919.

(35) Rizzi, A. C.; Piro, O. E.; Castellano, E. E.; Nascimento, O. R.; Brondino, C. D. *Inorg. Chim. Acta* **2000**, *305*, 19−25.

(36) Brondino, C. D.; Casado, N. M. C.; Passeggi, M. C. G.; Calvo, R. *Inorg. Chem.* **1993**, *32*, 2078−2084.

(37) Bencini, A.; Benelli, C.; Gatteschi, D.; Zanchini, C. *Inorg. Chem.* **1979**, *18*, 2137−2140.

(38) Bencini, A.; Benelli, C.; Gatteschi, D.; Zanchini, C. *Inorg. Chem.* **1980**, *19*, 1301−1304.

(39) Bencini, A.; Benelli, C.; Gatteschi, D.; Zanchini, C. *Inorg. Chem.* **1980**, *19*, 3027−3030.

(40) Brondino, C. D.; Calvo, R.; Atria, A. M.; Spodine, E.; Nascimento, O. R.; Peña, O. *Inorg. Chem.* **1997**, *36*, 3183−3189.

(41) Brondino, C. D.; Calvo, R.; Baran, E. J. *Chem. Phys. Lett.* **1997**, *271*, 51−54.

(42) Hilczer, W.; Goslar, J.; Tritt-Goc, J.; Hoffmann, S. K. *Inorg. Chem.* **1995**, *34*, 1852−1858.

(43) Reger, D. L.; Pascui, A. E.; Smith, M. D.; Jezierska, J.; Ozarowski, A. *Inorg. Chem.* **2012**, *51*, 7966−7968.

(44) Kahn, O. *Angew. Chem., Int. Ed. Engl.* **1985**, *24*, 834−850.

(45) Abragam, A.; Bleaney, B. *Electron paramagnetic resonance of transition ions*; Dover Publications: New York, 1986; p *xiv*, 911 pp.

(46) Bates, C.; Passeggi, M.; Stevens, K.; Wood, P. *J. Phys. C: Solid State Phys.* **1976**, *9*, 1511−1520.

(47) Zheng, Y.-Q.; Xie, H.-Z. *J. Sol. State Chem.* **2004**, *177*, 1352−1358.

(48) Xu, W.; Zheng, Y. Q. *Z. Kristallogr. - New Cryst. Struct.* **2004**, *219*, 235−236.

(49) Nelson, D.; Ter Haar, L. W. *Inorg. Chem.* **1993**, *32*, 182−188.

(50) Kahn, O. *Molecular Magnetism*; VCH Publishers: New York, 1993.

(51) Weil, J. A., Bolton, J. R. *Electron Paramagnetic Resonance*, 2nd ed.; John Wiley & Sons: Hoboken, NJ, 2007.

(52) Šebová, M.; Joríк, V.; Moncoľ, J.; Kožíšek, J.; Boča, R. *Polyhedron* **2011**, *30*, 1163−1170.

(53) Titiš, J.; Hudák, J.; Kožíšek, J.; Krutošíková, A.; Moncol, J.; Tarabová, D.; Boča, R. *Inorg. Chim. Acta* **2012**, *388*, 106−113.

(54) Garstens, M. A.; Singer, L. S.; Ryan, A. H. *Phys. Rev.* **1954**, *96*, 53−56.

(55) Pilbrow, J. R. *J. Magn. Reson.* **1978**, *31*, 479−490.

(56) Hagen, W. R. *Biomolecular EPR spectroscopy*; CRC Press: Boca Raton, FL, 2008; p 264.

(57) Werth, M. T.; Tang, S.-F.; Formicka, G.; Zeppezauer, M.; Johnson, M. K. *Inorg. Chem.* **1995**, *34*, 218−228.

(58) Pilbrow, J. R. *Transition Ion Electron Paramagnetic Resonance*, 1st ed.; Oxford University Press: New York, 1990; p 717.
(59) Zhang, K.-L.; Xu, Y.; You, X.-Z. *Transition Met. Chem.* **2005**, *30*, 376−379.